AIAA JOURNAL
Vol. 41, No. 7, July 2003

Titan IVB Linear-Shaped Charge Assembly Explosive Train Transfer Reliability

Lien C. Yang* and Ian P. H. Do†
Northrop Grumman Mission Systems Sector, San Bernardino, California 92402-1310

Detonation transfer in the end fitting of the linear-shaped charge assembly for flight termination destruct was quantitatively evaluated by using the CTH shock physics computer code pioneered by the Sandia National Laboratories. This critical transfer interface consists of a conic hexanitrostilbene transition charge used to boost the output of a reinforced confined detonating cord for the initiation of a ~1.59-g/cm (~750-grains/ft) cyclotetramethylene tetranitramine loaded and aluminum sheathed linear-shaped charge. These two elements are assembled together through an epoxy bond. As expected, the epoxy causes large shock pressure attenuations. However, for the worst-case epoxy thickness on the order of 3.81 mm (0.150 in.), adequate margin for reliable detonation transfer exists. Input geometry, mesh resolution, material properties, and output peak shock pressure/temperature spatial distributions are reported along with a brief description of the device history and design features. An artifact in the computation output is discussed for future improvement.

Nomenclature

P	=	shock pressure as a function of time at a given location, 10^{-1} GPa
P_1	=	P at the shock front, 10^{-1} GPa
R^2	=	coefficient of determination in the least-square straight line fit
T	=	shock temperature as a function of time at a given location, K
T_1	=	T at the shock front, K
t	=	time from artificial detonation of initiation pentaerythritol tetranitrate (PETN) explosive, μs
ΔT_1	=	temperature rise from the ambient at the shock front, K
ρ_0	=	normal density, g/cm^3
ρ_1	=	density at the shock front, g/cm^3
τ	=	shock pulse duration, μs

Introduction

THE design of the destruct charge for flight termination of the Titan IVB twin strapon solid rocket motor upgrade (SRMU) boosters adopts the state-of-the-art linear-shaped charge (LSC) technology.[1] There are a total of seven LSC assemblies (LSCAs) installed in the SRMU raceway in a linear array configuration with adjacent units interconnected by a short reinforced confined detonating cord (RCDC) explosive transfer system (ETS) to form a single continuous explosive train.[2] The LSCA in the forward SRMU segment is connected to a safe and arm (S&A) device in the nosecone section by an RCDC. On initiation, this LSCA and three each LSCAs on the middle and aft SRMU segments function to cut open all motor segments, thereby achieving the termination of SRMU propulsive thrust. The redundancy required for the high reliability is provided by a return ETS line also in the raceway consisting of three jointed long RCDCs routed from the end of the last aft segment LSCA to the redundant output port in the S&A.

The LSC contains 1.59 g/cm (~750 grains/ft) of ~1.77-g/cm^3 density cyclotetramethylene tetranitramine (HMX) explosive encased in an aluminum sheath. The 90-deg chevron shape of each ~3.05-m (~120-in.)-long individual LSC is formed through multiple extruding and swaging processes. The length of the LSC segment in each LSCA is ~2.08 m (~82 in.). Both segment ends are welded with a thin aluminum foil closure for a hermetic seal. Because the cross section of the LSC, ~1.57 cm (~0.620 in.) tall and ~1.88 cm (~0.740 in.) wide, is much larger than the endtip of RCDC, ~3.81 mm (~0.15 in.) in diameter, a truncated conic-shaped transition charge containing pressed hexanitrostilbene (HNS) explosive is designed for bridging these two elements to achieve a more uniform initiation of the LSC by the RCDC. This short cylindrical-shaped charge element is also welded with a thin stainless steel closure at each end. The assembly of the LSC end fitting is achieved by adding a threaded aluminum initiation block housing for RCDC installation, elastomer potting, aluminum LSC support/closure bushing, and epoxy. For the ensurance of intimate contact between the LSC and the transition charge, epoxy is also applied at this interface. The initiation blocks are in turn integrated with two mounting blocks to complete the assembly. (One block is for hard mount, and the other block is designed for sliding to offset motor case expansion during motor ignition.) Six mounting brackets located between the blocks provide additional support of LSCA for a designed standoff height of 3.18 cm (1.250 in.). The function requirement for the 100% LSC in-process-testing of cutoff end segments [~40.6 cm (~16 in.) long] is 1.37-cm (0.539-in.) minimum jet penetration and for LSCA is 1.27-cm (0.500-in.) average jet penetration, both measured by steel witness plates. This performance can be correlated to the total motor case severance with ample margin.

The LSCA was developed in the early 1990s. It was successfully qualified in accordance with range safety regulation requirements.[3] Four LSCA lots for 15 flight sets were successfully lot acceptance tested and delivered in support of launch operations. In 1999, the original HMX supplier, Holston Army Ammunition Plant, was not available for providing the material to fabricate a follow-on LSCA lot. HMX from a new supplier, Bofors Explosives in Sweden had to be used. HMX from both suppliers met the HMX specification, MIL-H-45444B (Ref. 4). However, substantial allowable differences in particle size distribution and crystal shape were observed. This explosive is considered the critical component in the LSCA. Changes of explosive characteristics usually require requalification. Modifications in the LSC manufacturing processes using the new HMX were successfully made to maintain its penetration performance. This approach was acceptable because the LSC end segments are

Presented as Paper 2001-3220 at the AIAA/ASME/SAE/ASEE 37th Joint Propulsion Conference, Salt Lake City, UT, 8–11 July 2001; received 31 December 2001; revision received 20 January 2003; accepted for publication 11 March 2003.

*Senior Staff Engineer, Propulsion, Structures and Fluid Mechanics Technical Center, Missile Defense Division, 1475 East Harry Sheppard Boulevard. Senior Member AIAA.

†Member, Technical Staff, Propulsion, Structures, and Fluid Mechanics Technical Center; currently Staff Scientist, Software Development Department, Livermore Software Technology Corporation, 7374 Las Positas Road, Livermore, CA 94550.

100% function tested for each LSC, and the LSCA lot acceptance test uses the same LSCA qualification environments per Ref. 3. However, the impact on the LSCA end fitting explosive train transfer reliability was uncertain. The interface between the RCDC endtip and the transition charge is the same as before. However, the statistical performance in the interface between the transition charge and the LSC end loaded with the HMX from the new supplier is not known with confidence. It is function tested in the LSCA lot acceptance tests but only involved a small sample size of 18 out of 89 units in the first LSCA lot made from the new HMX.

Traditionally, per Ref. 3, the reliability of explosive train transfer is demonstrated by firing tests using a gap that is at least four times the maximum allowable design gap, that is, drawing tolerances, which is 0.762 mm (0.030 in.) for the case of transition charge to LSC interface filled with epoxy or a 3.81-mm (0.15-in.) gap, whichever is greater. This type of testing is elaborate and expensive but was successfully performed early on in the LSCA development phase. It was decided to assess this problem analytically because it was generally recognized by the explosives community that ample margin may exist that can be quantified by analysis. This paper summarizes the results of the analysis using Sandia National Laboratories developed CTH shock physics computer code, which we previously used successfully in modeling the detonating cord endtip transfer.[2,5,6] A detailed analysis was also performed by The Aerospace Corporation using an alternate computer code. Both analyses confirmed the large margin for transfer reliability.

Background

The single most relevant parameter in the detonation transfer (or initiation) has been well established to be the pressure at the shock (or detonation) front. Early work[7] indicated that the threshold of successful transfer/initiation of high explosive also depends on the shock pulse duration. This knowledge was solidified in the studies of deflagration to detonation transition in the 1970s as the "$P_1^2\tau$ criterion" for the onset of successful transition, where P_1 is the shock front pressure and τ is the shock pulse duration.[8] It is an important criterion in the detonation initiation by a thin flyer plate mechanism in which the duration of inertial confinement is important. However, for our case of detonation transfer, because the variability in the pulse width is relatively small, as a first approximation, the key parameter is the peak shock pressure. Ample data in threshold transfer/initiation shock pressure exist for various high explosives at different porosities and particle sizes.[9–11] Unfortunately, very few data are available for the attenuation in epoxies. It is well known that the attenuation in hard materials, for example, glass and steel of small thickness to diameter ratio is insignificant.[12] In soft materials, for example, brass, aluminum, and Lucite, significant attenuation occurs. Ironically, the sensitivities established in Refs. 9–11 were obtained by using these materials of variable thickness as attenuators to obtain the different input shock pressure into the explosives under study, that is, the gap test. One report did provide shock attenuation in C-7 epoxy.[13] However, the maximum shock pressure used in the test was only 4.2 GPa, a level much lower than that required in our study. In addition, the tests there were performed by flyer plates; therefore, the results are not directly applicable to the current problem.

CTH Model

Background information for the CTH computer code can be found in Refs. 2, 5, 6, and 14. The following discussions are focused on the assumptions, applications, and limitations pertinent to our case study only.

Cases Under Study

Because of the intrinsic complex calculations in CTH and the fine resolutions required by our small thickness geometry, the computations were very time consuming. A typical run took approximately five full days of CPU time. (The computer was a Pentium II 450-MHz, 256-MB RAM, as reported in Ref. 2.) Therefore, besides the test runs for troubleshooting, only three cases were run for the evaluation of the detonation transfer efficiency:

1) Case 1 is 0.762-mm (0.030-in.)-thick epoxy between the transfer charge and the LCS end. This is the maximum allowed gap width per the LSCA drawing despite that, in the real implementation, the gaps are much smaller as shown in the neutron-radiographic inspection.

2) Case 2 is 3.05-mm (0.120-in.)-thick epoxy between the transfer charge and the LSC end. This is four times the maximum allowable gap width per the requirement of Ref. 3.

3) Case 3 is 3.05-mm (0.120-in.)-thick rubber between the transfer charge and the LSC end. This case was chosen as a better worst-case illustration over the 3.81-mm (0.150-in.)-thick gap required by Ref. 3 because 3.81-mm (0.150-in.)-thick epoxy results can be extrapolated from the 0.762-mm (0.030 in.)- and 3.05-mm (0.120-in.)-thick epoxy results, and it is well known that the rubber is more shock attenuative than the epoxy (as will also be indicated by our results).

Geometrical Input

The two-dimensional CTH code available to us cannot be applied to the three-dimensional configured chevron-shaped LSC. A circular cylindrical HMX charge has to be assumed. Two worst-case conditions were adopted to offset this potentially overly robust configuration: 1) the HMX density of 1.88 g/cm^3, the maximum theoretical density of HMX, is used in the model for HMX in LSC and 2) only a very thin aluminum wall of ~0.1 mm (~0.004 in.) is used to surround the HMX. This would make the propagation in HMX more difficult due to the high HMX density and the lack of a rigid confinement.

Figure 1 is a schematic diagram of the model for the case of 0.762-mm (0.030-in.)-thick epoxy; similarly, Fig. 2 is a schematic diagram of the model for the case of 3.05-mm (0.120-in.)-thick epoxy, which is identical to that for the case of 3.05-mm (0.120-in.)-thick rubber. Figures 3, 4, and 5 are the material legend diagrams for 0.762-mm (0.030-in.)-thick epoxy, 3.05-mm (0.120-in.)-thick epoxy, and 3.05-mm (0.120-in.)-thick rubber, respectively. Note, in Fig. 5, the same type of rubber is modeled for the rubber between the transition charge and the LSC and that which surrounds the LSC

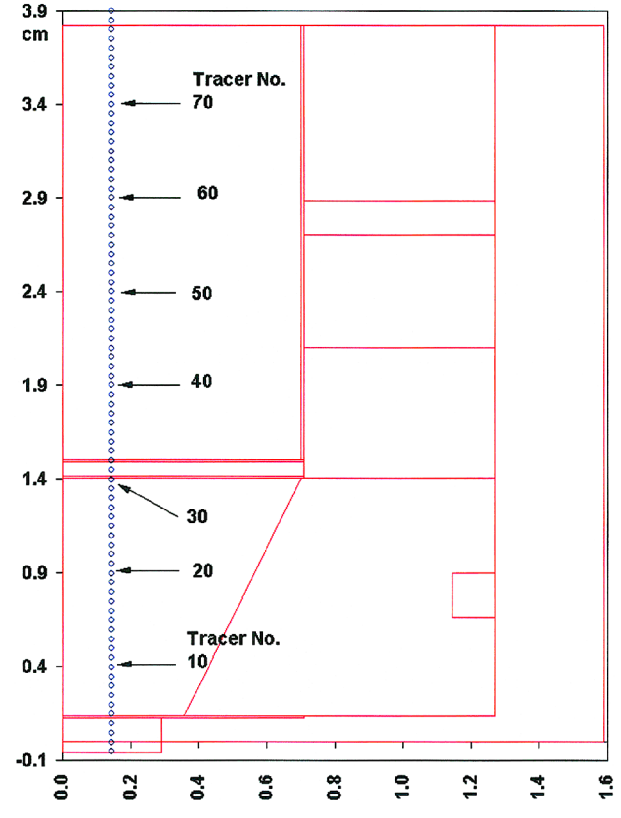

Fig. 1 LSCA end fitting geometry and tracer definition for 0.762-mm-(0.030-in.)-thick epoxy barrier.

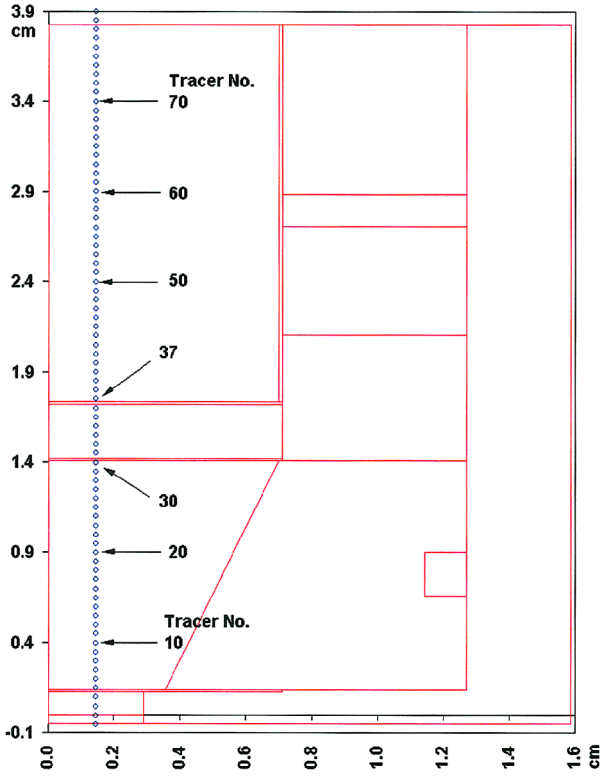

Fig. 2 LSCA end fitting geometry and tracer definition for 3.05-mm (0.120-in.)-thick epoxy barrier.

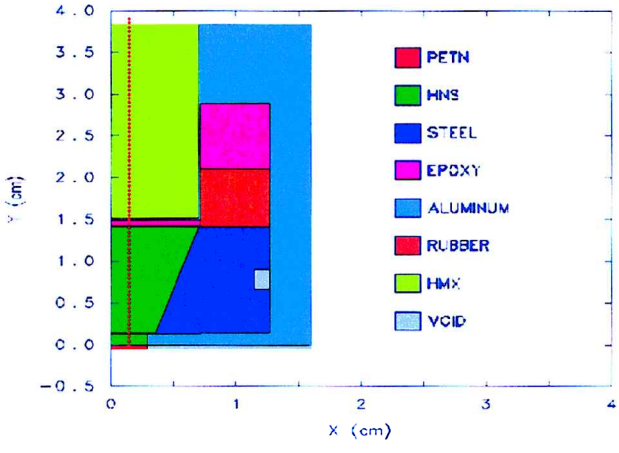

Fig. 3 Material legend in 0.762-mm (0.030-in.)-thick epoxy case study.

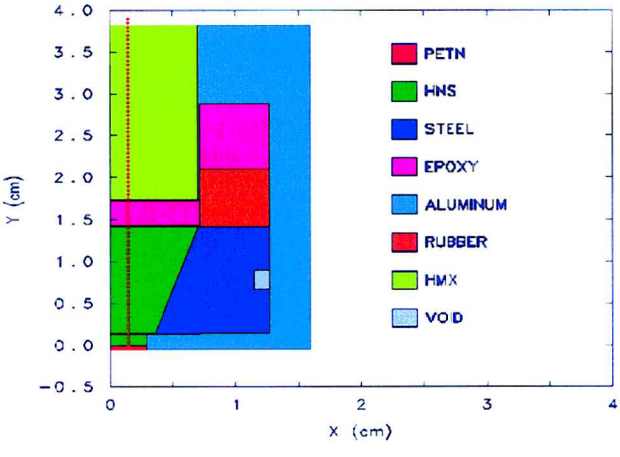

Fig. 4 Material legend in 3.05-mm (0.120-in.)-thick epoxy case study.

Table 1 Dimensions of local rectangular cells used in the mesh calculation

Location	Dimension, μm
Initiation PETN and HNS	23×10
Transition charge HNS	23×20
Thin closure disks	20×10
Epoxy or rubber between LSC and transition charge	23×10
LSC side wall	20×30
Upstream HMX	23×30
Downstream HMX	23×86
Transition charge housing	88×31
Aluminum housing, rubber and epoxy surrounding the LSC	88×30–86

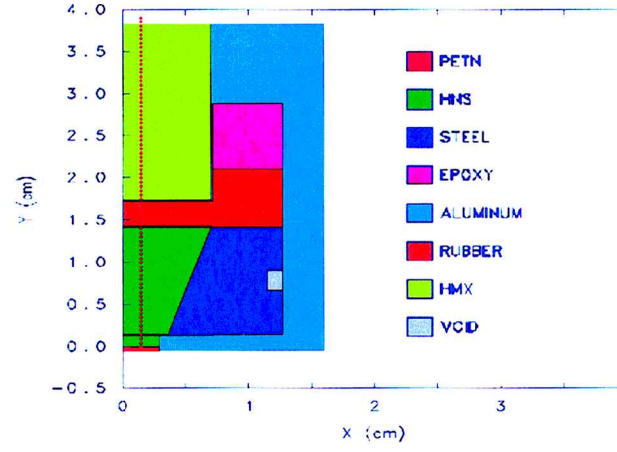

Fig. 5 Material legend in 3.05-mm (0.120-in.)-thick rubber case study.

and the steel body of the transition charge. In Figs. 3 and 4, the same type of epoxy is modeled for the epoxy between the transition charge and the LSC and that which surrounds the LSC.

Following a standard CTH approach, a 0.5-mm-thick 1.77-g/cm^3 density pentaerythritol tetranitrate (PETN) pellet is artificially detonated at $t = 0$ to start the detonation of the explosive train. It in turn detonates a 1.27-mm.-thick, 1.60-g/cm^3-density HNS increment simulating the RCDC endtip. The shock then passes through a 0.1-mm (0.004 in.)-thick steel closure disk on the transition charge and enters the 1.60-g/cm^3-density HNS loaded conic transition charge, which is encased in the steel charge holder. It then enters into the epoxy or rubber layer via a 0.1-mm (0.004-in.)-thick steel closure disk on the output end of the transition charge. It then enters into the 1.88-g/cm^3 HMX in the simulated LSC via a 0.1-mm (0.004-in.)-thick aluminum closure disk on the LSC input end. This end of the LSC is surrounded by ring-shaped rubber and epoxy potting compounds, as already described. Finally, the entire end hardware is encased in the aluminum initiation block and capped with an aluminum bushing (with a round hole opening to fit the simulated LSC) and potted with epoxy.

Only one-half of the LSCA end fitting is represented in the diagrams because of symmetry. A row of equally spaced discrete tracers are installed 3 mm away from the centerline to sample the time history of local shock parameters. At the resolution of the diagrams, the 0.1-mm (0.004-in.)-thick closure disks and simulated thin LSC sidewall are not quite visible, but they were included in the analysis.

Mesh Resolution

To conserve the total time that was required for the computation run, the mesh resolutions were allocated in accordance with the criticality of information and the dimension of the structure. The approximate cell dimensions (X and Y) were as given in Table 1.

The separation distance between two adjacent tracers was 0.493 mm.

Table 2 Material properties for CTH input

Material	EOS	CE
PETN	JWL[a] PETN4	Al, JC[b] 7
HNS	HVRB[c] HNS-I	Al, JC 7
HMX	HVRB HMX	AI, JC 7
Steel	Sesame steel	Steel, JC 9
Epoxy	Sesame epoxy	Al, JO[d] 7
Aluminum	Sesame aluminum	Al, JO 7
Rubber	Sesame nylon	Polyethersulfon, JO 14

[a]Jones–Wilkins–Lee.
[b]Johnson and Cook.
[c]History variable reactive burn.
[d]Johnson.

Material Properties

The equation of state (EOS) and constitutive equation (CE), available from CTH files for the materials used in the simulation are summarized in Table 2. (In CTH code, initials of data originators and acronyms are used as programming identifications in the material property database files.)

Highlights of Result

General Descriptions

Figures 6 and 7 show the time frames of pressure and temperature distribution of all three cases at times of interest: just before the shock front entering the epoxy or rubber, during the shock front residence in the epoxy or rubber, shock front just exiting the epoxy

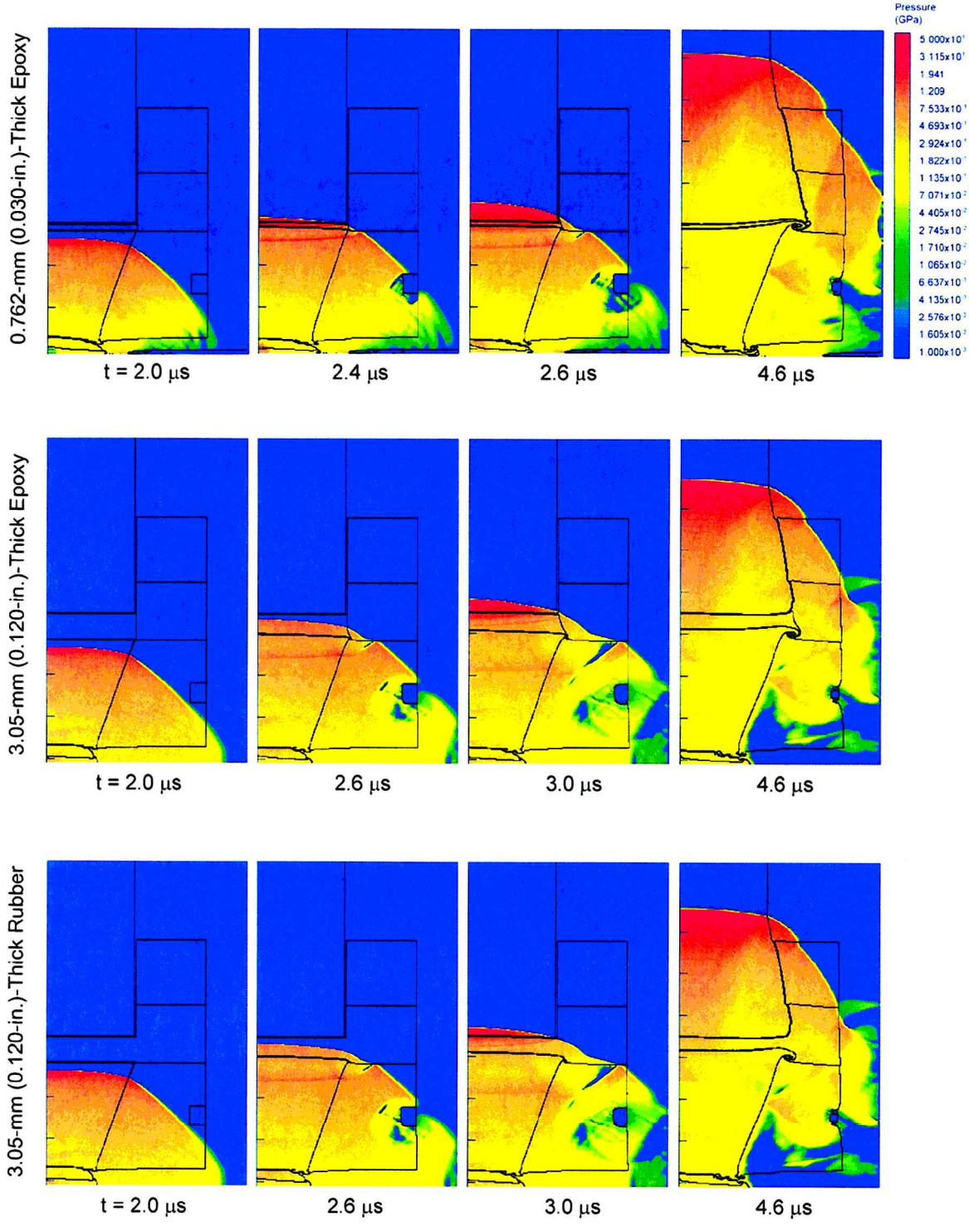

Fig. 6 Selected pressure distribution time frames for all three cases.

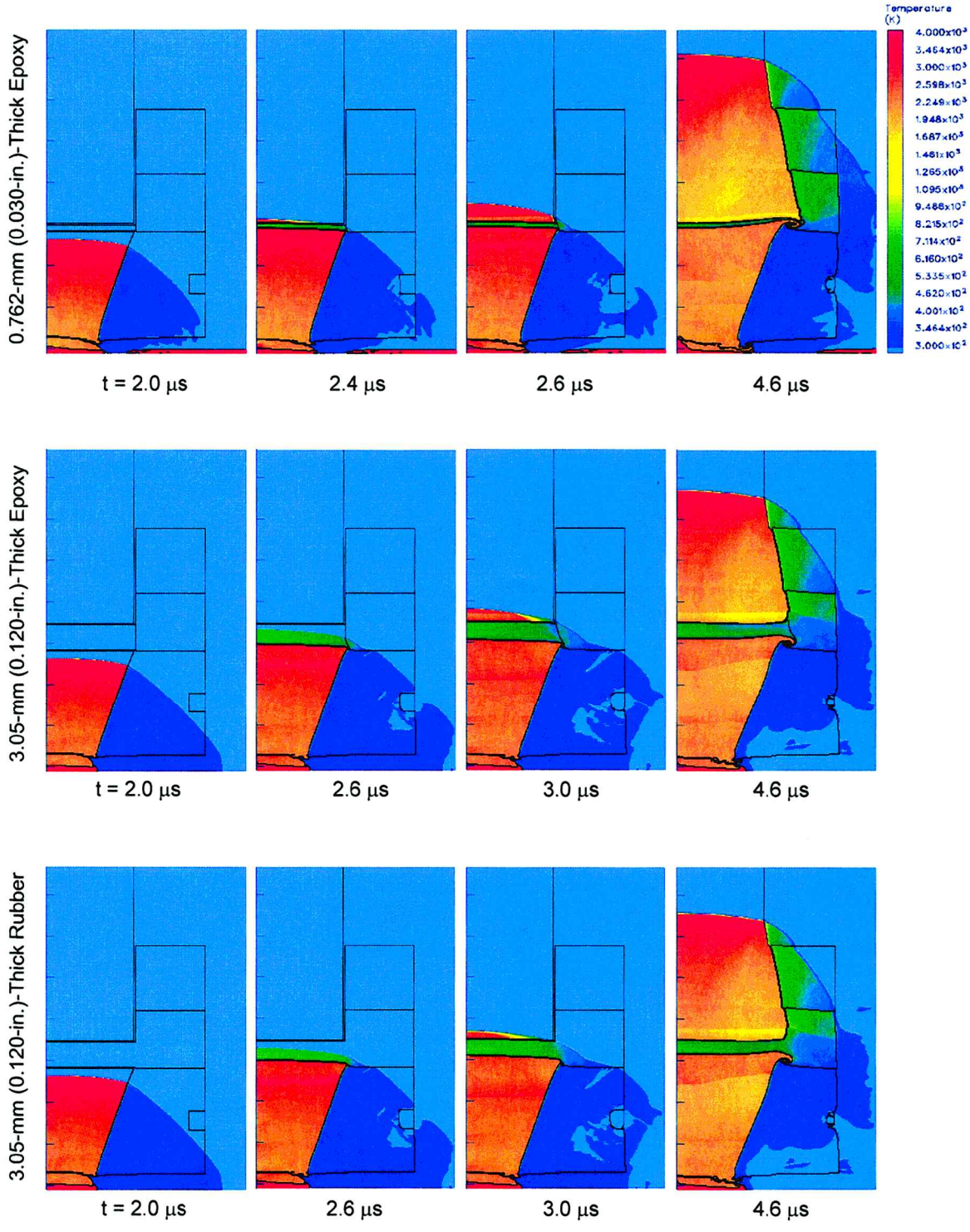

Fig. 7 Selected temperature distribution time frames for all three cases.

or rubber, and shock front nearly passing through the LSC end fitting. The shock front shape and the distortion of materials surrounding the explosion were essentially the same for all three cases, except the different time delays introduced by the different inert material or thickness, as expected. This indicates that no significant impact was introduced by interruption of the explosive train. According to Gibbs and Popolato,[11] at the shock initiation threshold of 4.41 GPa for 1.88-g/cm^3-density HMX, slower shock velocities and longer run distances on the order of 4.12 mm/μs (about 45.2% of steady state value) and 7.74 mm would result and should be notable in the figures if they existed. Therefore, the absence of these indications implies that the shock pressures after passing through the epoxy or rubber barrier were much higher than the 4.41 GPa threshold.

Quantitative Local Shock Front Pressure Data

Figures 8–12 show the pressure–time history profiles at tracers 30, 31, 35, 37, and 40 for the case study of 3.05-mm (0.120-in.)-thick epoxy. It can be seen that the shock front pressure decreased drastically from 29.0 to 15.0 GPa immediately after it entered the epoxy. Then it further decreased at a slower rate as a function of the penetration distance into the epoxy. It rapidly recovered to a higher value of 45.8 GPa, roughly corresponding to the detonation pressure of the 1.88-g/cm^3-density HMX at tracer 40, which was merely 1.5 mm from the LSC entrance interface. The sharp rise time of the pressure was maintained in the epoxy, but some pulse broadening and emergence of multiple peaks after the initial shock front passing were observed.

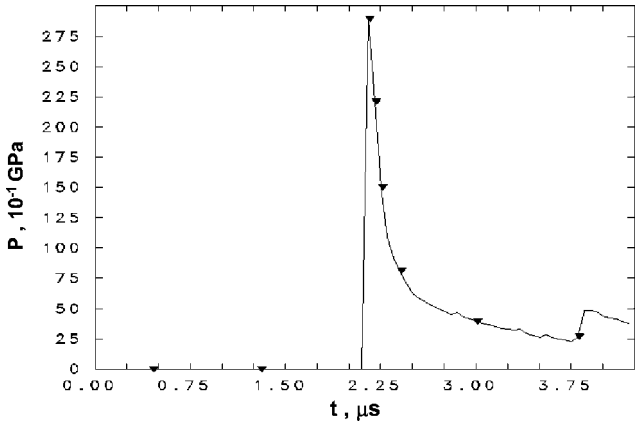

Fig. 8 Shock pressure time profile at tracer 30 in 3.05-mm (0.120-in.)-thick epoxy case study.

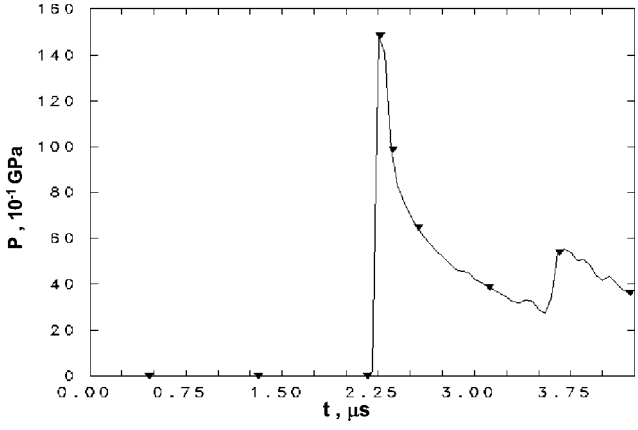

Fig. 9 Shock pressure time profile at tracer 31 in 3.05-mm (0.120-in.)-thick epoxy case study.

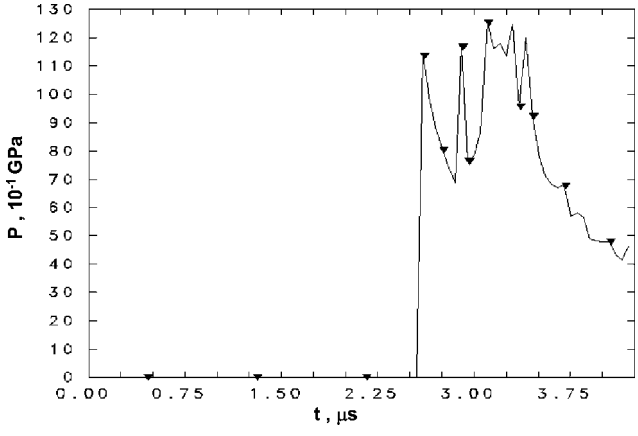

Fig. 10 Shock pressure time profile at tracer 35 in 3.05-mm (0.120-in.)-thick epoxy case study.

Figures 13–15 show the spatial profile of the peak shock pressure for the three cases. Both decreases in peak shock pressure in the inert material and a rapid reestablishment of high-order detonation in HMX can be seen. As expected, the shock attenuation in the rubber is stronger than in the epoxy. The margin of the transfer reliability is indicated by the ratio of shock front pressure input to HMX in the LSC at the last tracer in the inert layer just in front of the inert-layer/LSC interface, to the HMX shock initiation threshold, 4.41 GPa. The results are summarized in Table 3.

From the results, it can be concluded that adequate margins exist for all four cases listed. Failure in transfer could be predicted if the

Table 3 Detonation transfer reliability

Case	Shock front pressure input to LSC, GPa	Ratio to 4.41-GPa HMX shock initiation threshold
0.762-mm (0.030-in.)-thick epoxy	14.98 (tracer 31)	3.40
3.05-mm (0.120-in.)-thick epoxy	10.42 (tracer 36)	2.36
3.05-mm (0.120-in.)-thick rubber	8.02 (tracer 36)	1.82
3.81-mm (0.150-in.)-thick epoxy	8.50 (extrapolated)	1.93

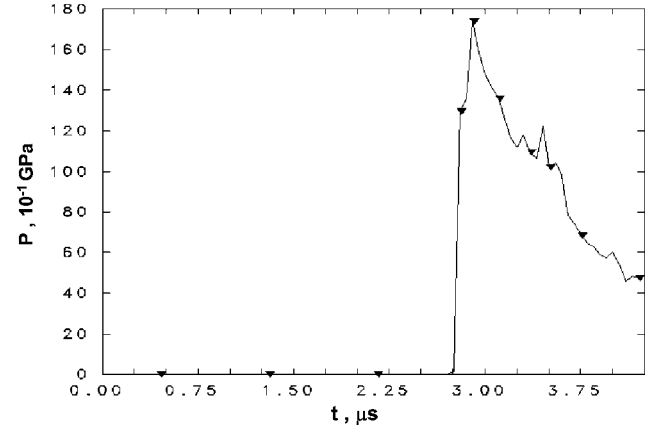

Fig. 11 Shock pressure time profile at tracer 37 in 3.05-mm (0.120-in.)-thick epoxy case study.

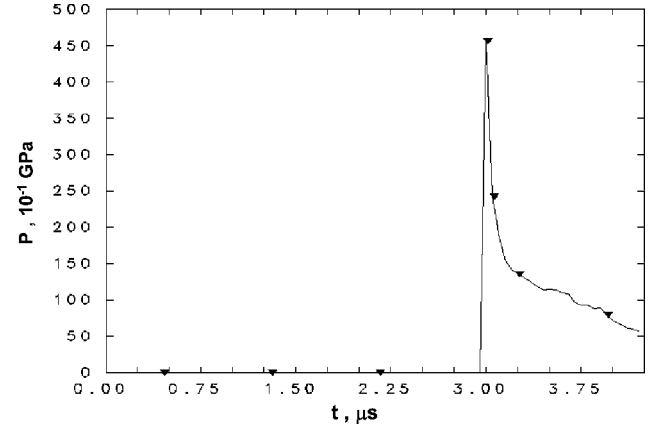

Fig. 12 Shock pressure time profile at tracer 40 in 3.05-mm (0.120-in.)-thick epoxy case study.

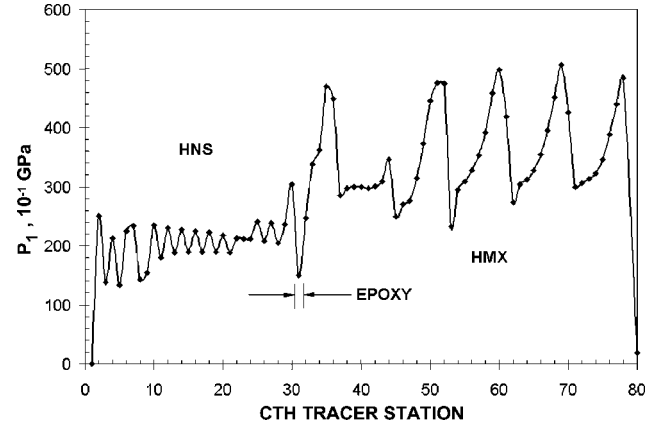

Fig. 13 Detonation transfer in LSCA end fitting via 0.762-mm (0.030-in.)-thick epoxy, shock front pressure vs location.

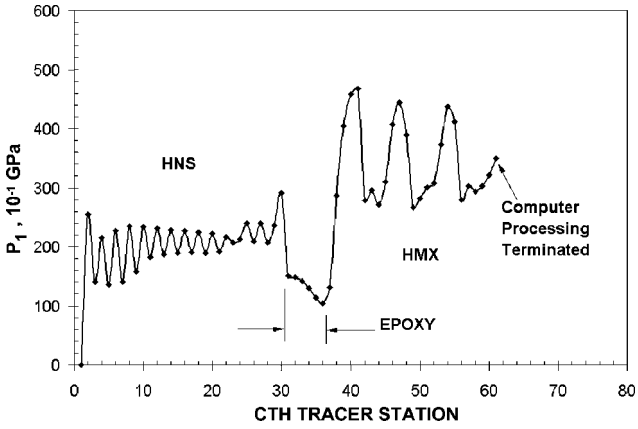

Fig. 14 Detonation transfer in LSCA end fitting via 3.05-mm (0.120-in.)-thick epoxy, shock front pressure vs location.

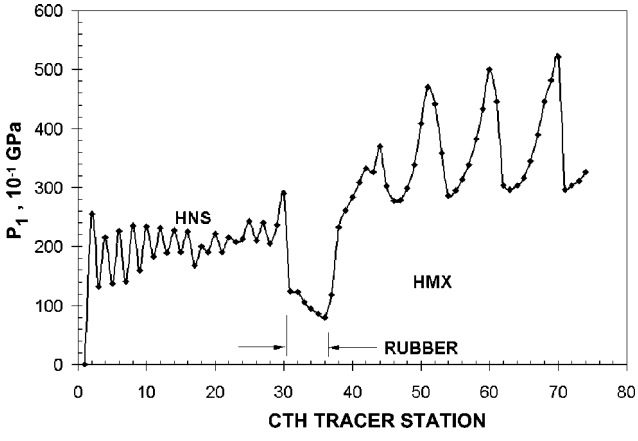

Fig. 15 Detonation transfer in LSCA end fitting via 3.05-mm (0.120-in.)-thick rubber, shock front pressure vs location.

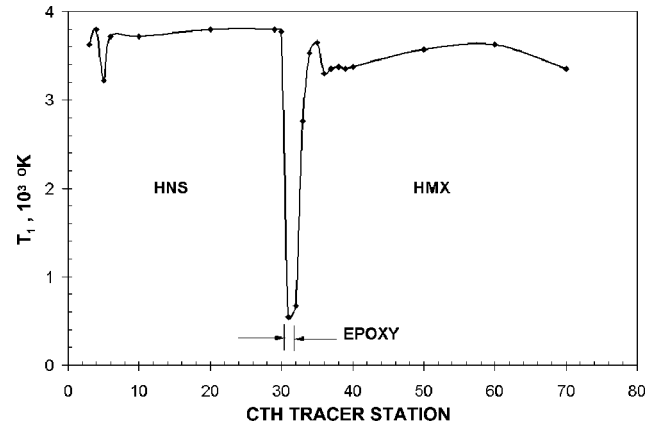

Fig. 16 Detonation transfer in LSCA end fitting via 0.762-mm (0.030-in.)-thick epoxy, shock front temperature vs location.

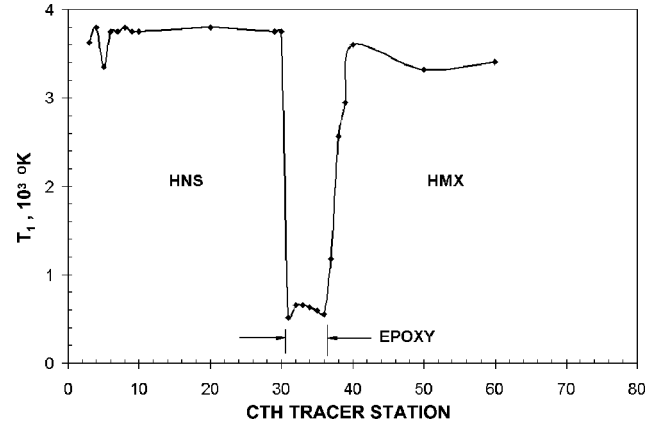

Fig. 17 Detonation transfer in LSCA end fitting via 3.05-mm (0.120-in.)-thick epoxy, shock front temperature vs location.

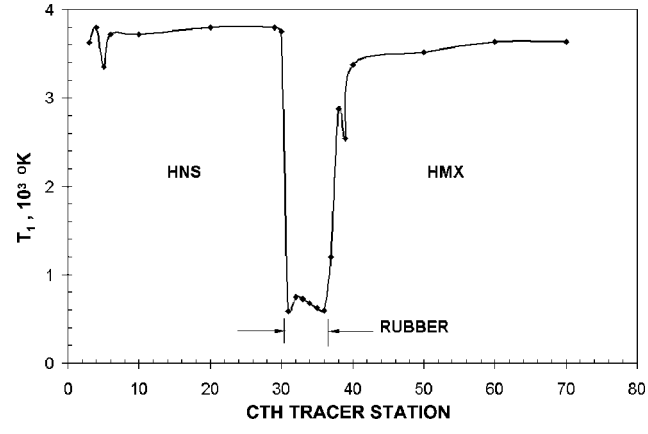

Fig. 18 Detonation transfer in LSCA end fitting via 3.05-mm (0.120-in.)-thick rubber, shock front temperature vs location.

thickness of the epoxy and/or rubber is further increased beyond ~6.35 mm (~0.250 in.).

Discussion

The large oscillatory variation in the shock front pressure at different tracer locations shown in Figs. 13–15 needs be addressed. This phenomenon is present in both HNS and HMX. The variation in HNS appears to be periodic with a spacing of two tracers and with an average value of ~20.0 GPa, the detonation pressure of the 1.6-g/cm^3-density HNS according to the CTH database. The variation in HMX appears to be periodic with a spacing of six tracers and with an average value of ~35.5 GPa, ~10% below 39.5 GPa, the detonation pressure of the 1.88-g/cm^3-density HMX (Ref. 11). The variation is considered as an artifact generated by the calculation, because the ~50.0 GPa of shock front pressure in HMX is unreal as it deviates considerably from the database value of 39.5 GPa for the 1.88-g/cm^3-density HMX.

The phenomenon is not introduced by the interruption by the inert barriers because the variations observed in HMX were essentially the same for all three cases, which have different barrier material and barrier thickness. It does not appear to be affected by the mesh size selection because the same variation was observed in both upstream HMX and downstream HMX, which have approximately a factor of three difference in Y-axis mesh width. The oscillatory behavior of shock front pressure is seen in both explosive materials, HNS and HMX. However, Figs. 13–15, which plot the shock front pressure vs tracer locations for three sample cases, do not indicate any oscillatory pressure pattern in the inert materials, epoxy and rubber. This seems to indicate that the cause of this computational artifact may likely be in the explosive-burn routine. It may be of interest to apply different burn models, such as Arrhenius burn, ignition and growth reactive burn, and forest fire reactive burn for further investigations.

Similar variations were also observed in other shock front parameters, for example, the density and particle velocity at the shock front. This is an expected result because these two parameters are closely related to the peak shock pressure. Figures 16–18 show the temperature at the shock front as a function of tracer location for the three cases under study. It appears that the temperature at the shock front does not exhibit any significant variations at different

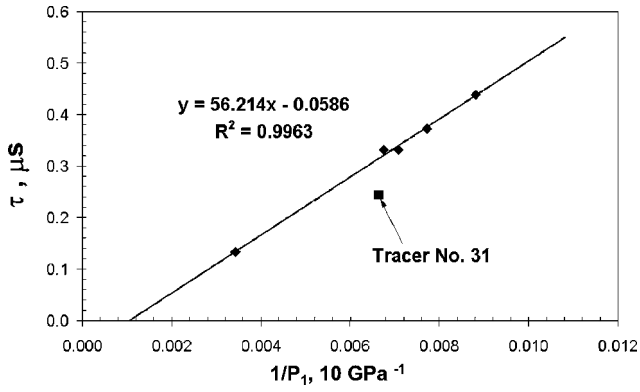

Fig. 23 FWHM shock pulse width as an inverse function of shock front pressure in 3.05-mm (0.120-in.)-thick epoxy case study.

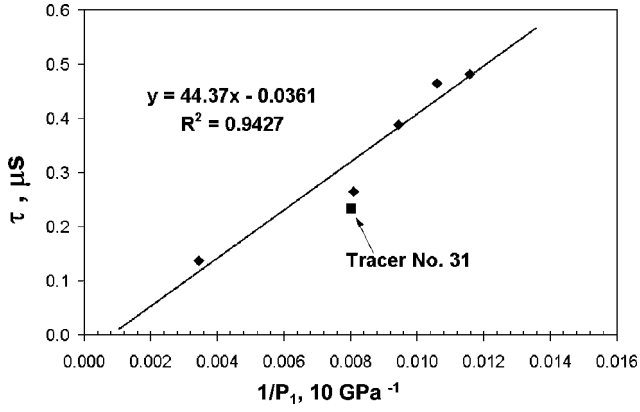

Fig. 24 FWHM shock pulse width as an inverse function of shock front pressure in 3.05-mm (0.120-in.)-thick rubber case study.

Epoxy:

$$\tau = 56.214P_1^{-1} - 0.0586, \qquad R^2 = 0.9963 \tag{4}$$

Rubber:

$$\tau = 44.370P_1^{-1} - 0.0361, \qquad R^2 = 0.9427 \tag{5}$$

For the completeness of information, the densities at shock front, ρ_1, of epoxy and rubber as a function of shock front pressure are presented in the following straight-line fit equations with the intercepts at $P_1 = 0$ least-square preset at $\rho_0 = 1.38$ g/cm^3 and 1.14 g/cm^3 for epoxy and rubber, respectively.

Epoxy:

$$\rho_1 = 0.0052P_1 + 1.38, \qquad R^2 = 0.9831 \tag{6}$$

Rubber:

$$\rho_1 = 0.0067P_1 + 1.14, \qquad R^2 = 0.9513 \tag{7}$$

Reverse Propagation

The transfer reliability in the inverse direction, that is, from HMX in LSC to HNS in the transition charge, is of equal importance. This case was not simulated due to one quite transparent reason. Assuming the percentage of attenuations of the peak shock pressure in the epoxy and rubber are the same in the reverse direction, the 39.50-GPa shock front pressure in HMX would warrant a minimum of 15.84 GPa of shock front pressure exiting the epoxy for the initiation of the HNS, a level close to the detonation pressure of HNS, that is, 20.0 GPa. Therefore, successful transfer is a certainty. In addition, the conic geometry may impose a focusing effect on the shock, which would further enhance the transfer reliability.

Summary

1) The CTH shock physics computer code successfully characterized two categories of important cases in shock physics applicable to our case studies: a) shock attenuation in inert plastic/elastomer material, such as epoxy and rubber, and b) initiation of an insensitive high explosive by the shock exiting from the inert material. The predictions are consistent with the known database; therefore, it can serve as a quantitative assessment for transfer reliability in lieu of elaborate and expensive testing. This has been a primary objective of CTH, and in our case, it is indeed well served.

2) For the specific problem of interest, the detonation transfer reliability in the Titan IVB LSCA end fitting, which consists of HNS and HMX buffered with a layer of epoxy, has been successfully demonstrated. For the worst-case epoxy thickness of 3.81 mm (0.15 in.) and HMX with theoretical maximum density of 1.88 g/cm^3, a margin factor of 1.93 was obtained, which is consistent with a high reliability for components in a flight termination system. The result is independent of HMX porosity, particle size, and crystalline shape because the worst-case TMD was used for the evaluation.

3) Temperature rise in inert material under shock loading as a linear function of shock pressure has been formulated. A $P_1\tau = \text{const}$ relationship is found, which is consistent with the $P_1^2\tau$ shock energy dissipation theory and implies a shock pressure pulse broadening as a result of shock propagation and energy dissipation in the plastic/elastomer material.

4) A computation related artifact, that is, the peak shock pressure oscillatory variation as a function of location, has been identified, and possible strategies for further work are discussed.

Acknowledgments

The writers acknowledge their colleagues of the Titan IV solid rocket motor upgrade ordnance team for discussions and providing model input information used in the paper: D. R. Lee and G. Dougherty of Goodrich, Inc.; J. York and W. Thorup of Alliant Techsystems, Inc.; D. L. Jackson of Lockheed Martin Aerospace Co.; S. Goldstein, L.H. Horwitz and A. O. Lopez of The Aerospace Corporation; U.S. Air Force Range Safety officers M. Gotfraind of Western Range at Vandenberg Air Force Base and S. Phoonkeao of Eastern Range at Cape Canaveral Air Force Station; J. Eisenreich of the U.S. Air Force Space and Missile Systems Center; and M. Dao-Randall, B. G. Morton, and D. P. Moore of Northrop Grumman, Inc.

References

[1]Brauer, K. O., *Handbook of Pyrotechnics*, Chemical Publishing, New York, 1974, pp. 11–12, 373–375.

[2]Yang, L. C., Do, I. P. H., and McMunn, J. C., "Confined Detonating Cord Blowout Analysis," AIAA Paper 2000-3734, July 2000.

[3]Range Safety Office, *Airborne Range Safety System Documentation, Design and Test Requirements*, Eastern and Western Range 127-1, Vol. 2, Patrick AFB, FL, 1993, Chap. 4.

[4]"Military Standard, HMX," MIL-STD MIL-H-45444B, U.S. Army Armament Research Development Command, Dover, NJ, Feb. 1974.

[5]Yang, L. C., and Do, I. P. H., "Key Parameters for Controlling of Function Reliability in 'Nonel Tube' Explosive Transfer System," AIAA Paper 99-2420, June 1999.

[6]Yang, L. C., and Do, I. H. P., "Nonelectrical Tube Explosive Transfer System," *AIAA Journal*, Vol. 38, No. 12, 2000, pp. 2260–2267.

[7]Gittings, E. F., "Initiation of a Solid Explosive by a Short-Duration Shock," *Proceeding of Fourth Symposium (International) on Detonation*, ACR-126, Office of Naval Research, Department of the Navy, Washington, DC, 1965, pp. 373–380.

[8]Walker, F. E., Cowperthwaite, M., Frey, R., Howe, P., Mader, C., and Fauquignon, C., "Discussion on Shock Initiation and $P^2\tau$," *Proceedings of Sixth Symposium (International) on Detonation*, ACR-221, Office of Naval Research, Department of the Navy, Washington, DC, 1976, pp. 82–94.

[9]Scott, C. L., "Effect of Particle Size on Shock Initiation of PETN, RDX and Tetryl," *Proceedings of Fifth Symposium (International) on Detonation*, ACR-184, Office of Naval Research, Department of the Navy, Arlington, VA, 1970, pp. 259–266.

[10]Bauer, R. J., "An Analysis of Small Scale Gap Test Sensitivity Data Using Porosity Theory and Nonreactive Shock Huguenots," Naval Surface Weapon Center, Rept. NSWC/WOL/TR 75-67, White Oak, MD, June 1975.

[11]Gibbs, T. R., and Popolato, A., *LASL Explosive Property Data*, Univ. of California Press, Berkeley, CA, 1980, pp. 48, 299, 300.

[12]Cook, M. A., *The Science of High Explosives*, Krieger, Malabar, FL, 1958, pp. 83–87.

[13]Erkman, J. O., "Elastoplastic Effects in the Attenuation of Shock Wave," *Proceedings of Fourth Symposium (International) on Detonation*, ACR-126, Office of Naval Research, Department of the Navy, Washington, DC, 1965, pp. 277–288.

[14]Hertel, E. S., Bell, R. L., Elrick, M. G., Farsworth, A. V., Kerley, G. I., McGlaun, J. M., Petney, S. V., Silling, S. A., Taylor, P. A., and Yarrington, L., "CTH, A Software Family for Multi-Dimensional Shock Physics Analysis," *Proceedings of the 19th International Symposium on Shock Waves*, Vol. 1, edited by R. Burn and L. D. Dumitrescu, Springer-Verlag, Berlin, 1995, pp. 377–382.

M. Sichel
Associate Editor

Color reproductions courtesy of Northrop Grumman, Inc.